Journal of Nuclear Materials 498 (2018) 458–467

Contents lists available at ScienceDirect

Journal of Nuclear Materials

journal homepage: www.elsevier.com/locate/jnucmat

Characterization of faulted dislocation loops and cavities in ion irradiated alloy 800H

Christopher J. Ulmer*, Arthur T. Motta

Department of Mechanical and Nuclear Engineering, The Pennsylvania State University, University Park, PA 16802, USA

ARTICLE INFO

Article history:
Received 12 June 2017
Received in revised form
7 November 2017
Accepted 8 November 2017
Available online 14 November 2017

Keywords:
Ion irradiation
Faulted loop
Cavity
800H
In-situ irradiation

ABSTRACT

Alloy 800H is a high nickel austenitic stainless steel with good high temperature mechanical properties which is considered for use in current and advanced nuclear reactor designs. The irradiation response of 800H was examined by characterizing samples that had been bulk ion irradiated at the Michigan Ion Beam Laboratory with 5 MeV Fe^{2+} ions to 1, 10, and 20 dpa at 440 °C. Transmission electron microscopy was used to measure the size and density of both {111} faulted dislocation loops and cavities as functions of depth from the irradiated surface. The faulted loop density increased with dose from 1 dpa up to 10 dpa where it saturated and remained approximately the same until 20 dpa. The faulted loop average diameter decreased between 1 dpa and 10 dpa and again remained approximately constant from 10 dpa to 20 dpa. Cavities were observed after irradiation doses of 10 and 20 dpa, but not after 1 dpa. The average diameter of cavities increased with dose from 10 to 20 dpa, with a corresponding small decrease in density. Cavity denuded zones were observed near the irradiated surface and near the ion implantation peak. To further understand the microstructural evolution of this alloy, FIB lift-out samples from material irradiated in bulk to 1 and 10 dpa were re-irradiated in-situ in their thin-foil geometry with 1 MeV Kr^{2+} ions at 440 °C at the Intermediate Voltage Electron Microscope. It was observed that the cavities formed during bulk irradiation shrank under thin-foil irradiation in-situ while dislocation loops were observed to grow and incorporate into the dislocation network. The thin-foil geometry used for in-situ irradiation is believed to cause the cavities to shrink.

1. Introduction

The development and use of advanced alloys in nuclear reactors is key to extending the lifetimes of components in current light water reactors and advanced reactor designs. Alloy 800H (UNS N08810) is an austenitic stainless steel that is often used in service up to 593 °C due to its good resistance to creep and rupture [1]. 800H is a high nickel steel with the chemical composition shown in Table 1. Austenitic stainless steels have been observed to undergo various microstructural changes during irradiation, including the formation of faulted dislocation loops, the development of a dislocation network, swelling by the nucleation and growth of cavities, and precipitation of second phases [2,3]. In order to utilize 800H in current and future reactors, these microstructural changes and their development in the reactor environment must be well understood, especially at high doses. Because of the long irradiation times required to achieve such high doses using neutron irradiation, ion irradiation is a useful tool to explore high damage regimes, as the dose rates typically achievable are orders of magnitude higher than those achievable with neutrons [4]. To achieve this goal, it is necessary to characterize ion irradiated microstructures and later benchmark the characterization by examining neutron irradiated samples.

Alloy 800H has been irradiation tested recently using both ion and neutron irradiation. Gan et al. found that faulted dislocation loops and fine precipitates formed in 800H after bulk ion irradiation to 5 and 50 dpa at 500 °C using 5 MeV Ni ions but observed no cavities [5]. Gan and Hilton also characterized 800H after neutron irradiation in the Advanced Test Reactor (ATR) to 1.3 dpa at 500 °C and 1.5 dpa at 800 °C and observed the formation of precipitates, both gamma prime and $M_{23}C_6$-type, and of small cavities with diameter on the order of a few nanometers [6]. Tan et al. found faulted dislocation loops, cavities and gamma prime precipitates in 800H irradiated to 3 dpa at 500 °C in the ATR [7]. Nanstad et al. used

* Corresponding author.
E-mail address: cju5002@psu.edu (C.J. Ulmer).

https://doi.org/10.1016/j.jnucmat.2017.11.012
0022-3115/

Table 1
Nominal chemical composition for alloy 800H [1].

	Fe	Ni	Cr	Mn	C	Cu	Si	S	Al	Ti
Max	–	35.0	23.0	1.5	0.10	0.75	1.0	0.015	0.60	0.60
Min	39.5	30.0	19.0	–	0.05	–	–	–	0.15	0.15

Table 2
Chemical composition (wt. %) as measured by Luvak Inc. for alloy 800H heat # 35175 supplied by G.O. Carlson Inc.

Fe	Ni	Cr	Mn	C	Cu	Si	S	Al	Ti
Bal.	30.9	20.3	0.74	0.075	0.36	0.16	0.001	0.56	0.34
O	N	H	Mo	Nb	P	W	V		
0.003	0.008	0.00033	0.065	0.004	0.007	0.009	0.039		

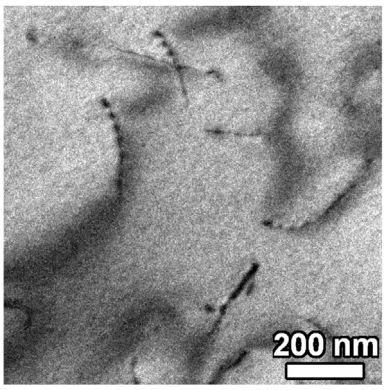

Fig. 1. Bright-field TEM micrograph ($g = 002$) showing the typical unirradiated microstructure of 800H.

tensile tests to measure the mechanical properties of 800H after neutron irradiation in the High-Flux Isotope Reactor (HFIR) to doses of 1.28 dpa and 1.61 dpa at 580 °C and 660 °C, respectively and found significant hardening at the lower irradiation temperature and a reduction of tensile elongation at both temperatures [8].

These past efforts focused on higher temperatures ($\geq$ 500 °C) than would be applicable to most advanced reactor designs. The current work seeks to expand this data to lower temperatures by irradiating 800H at a temperature of 440 °C using 5 MeV Fe^{2+} ions to low and intermediate doses of 1, 10 and 20 dpa. The faulted loop and cavity microstructure was methodically characterized as functions of depth from the irradiated surface to help understand the effects of the proximity of the surface, radiation dose, and ion implantation on the development of the microstructure. Finally, samples taken from bulk ion irradiated material, which already contained defects produced by irradiation, were re-irradiated in-situ to further help inform the mechanisms and dynamics of 800H microstructure evolution under irradiation.

2. Experiment

The 800H alloy was supplied by G.O. Carlson Inc. as heat # 35175. The alloy composition was measured by Luvak Inc. and is shown in Table 2. The grain size of the as-received material was approximately 200 μm, and the typical unirradiated dislocation microstructure is shown in Fig. 1. The samples contained most commonly $Cr_{23}C_6$ type carbides, with a few titanium carbides present. They were few in number, with the former observed to be intergranular and the latter intragranular. Their density was low enough that transmission electron microscope (TEM) samples often showed no precipitates.

Bulk ion irradiations were performed at the Michigan Ion Beam Laboratory in the context of an IRP project on the simulation of neutron irradiation using ion irradiation. Sample bars with dimensions 20 mm × 1.5 mm × 1.5 mm were prepared for irradiation by mechanical polishing to 0.02 μm finish followed by electropolishing. The samples were irradiated using a defocused beam of 5 MeV Fe^{2+} ions generated by a 3 MV Pelletron accelerator. Parallel neutron irradiations are performed with an expected nominal irradiation temperature of 380 °C, and as such these ion irradiations were performed at 440 °C for a temperature shift of 60 °C.[1] The sample temperature was monitored using an infrared camera and four thermocouples attached to the bar outside the irradiated region. Careful temperature control meant that the temperature during irradiation varied less than 5 °C (2σ).

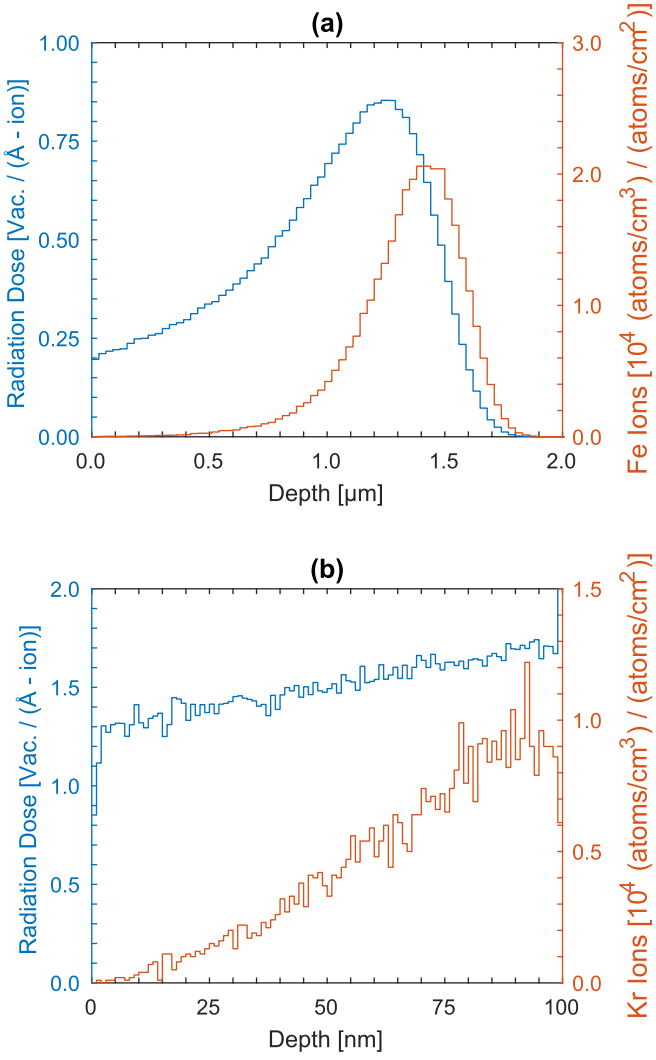

Fig. 2. The radiation damage and ion implantation depth profiles for (a) 5 MeV Fe^{2+} bulk ion irradiation and (b) 1 MeV Kr^{2+} in-situ ion irradiation of 800H as calculated using SRIM.

The ion fluence to dpa ratio was calculated using the Stopping and Range of Ions in Matter (SRIM) [10] Monte Carlo simulation

[1] We use Eq. (14) in Ref. [9] with a ratio of ion dose rate to neutron dose rate equal to 500, a vacancy formation energy of 1.5eV, and a vacancy migration energy of 1.2eV to calculate the temperature shift.

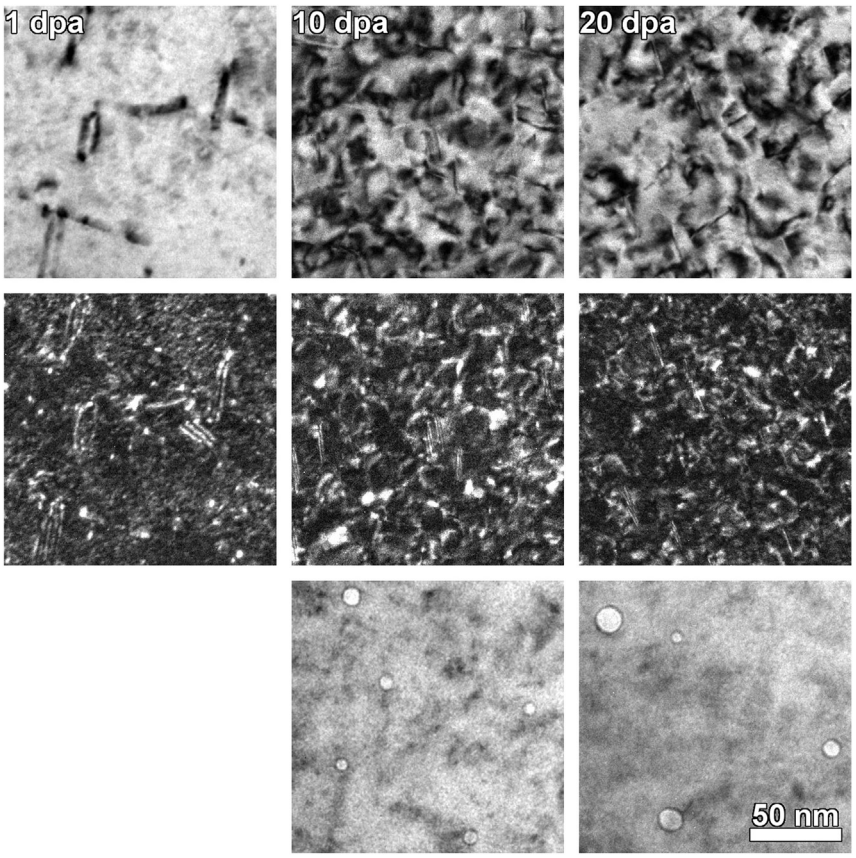

Fig. 3. TEM images of 800H after bulk ion irradiation to 1, 10, and 20 dpa at 440 °C. Top: Bright-field image with $g = 002$ diffraction condition near the 110 zone axis at 0.6 μm depth from the irradiated surface. Middle: Semi-weak beam dark-field images show the dislocation microstructure in greater detail. The images correspond to the same sample area as the corresponding bright-field images and were acquired with $g = 002$ (g, 4g) condition. Bottom: Underfocused TEM images show cavities that formed after bulk ion irradiation. No cavities were observed at 1 dpa.

software. The simulation was carried out using the "Ion Distribution and Quick Calculation of Damage" option and assumed a displacement energy of 40 eV, as recommended by Stoller [11]. The radiation damage and ion implantation profiles as functions of sample depth calculated from SRIM are shown in Fig. 2(a). A depth of 0.6 μm was chosen as the target for the characterization of irradiation induced defects because it is as far from the sample surface as possible while also avoiding the ion implantation peak. With this method, it was found that an ion fluence of 2.26×10^{19} ions/m^2 is equivalent to 1 dpa at 0.6 μm depth. Samples were irradiated to 1, 10 and 20 dpa at the target depth. The average damage rates were similar: 4.92×10^{-4} dpa/s, 4.50×10^{-4} dpa/s and 5.88×10^{-4} dpa/s for the three irradiation campaigns, respectively.

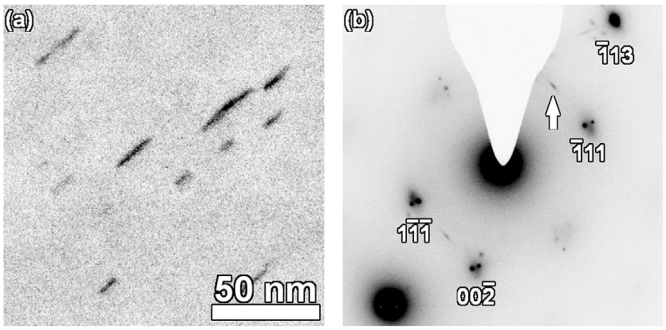

Fig. 4. (a) Rel-rod dark-field TEM image of edge-on faulted dislocation loops in 800H after bulk ion irradiation to 20 dpa at 440 °C. (b) The corresponding diffraction pattern that shows the rel-rod dark-field imaging condition. The arrow indicates the rel-rod used for imaging the faulted loops. The contrast is inverted for both images.

TEM lift-out samples were prepared from bulk ion irradiated material using in-situ lift-out in a focused ion beam (FIB). The surface was protected with initial electron beam deposited carbon layer and then ion beam deposited carbon. Milling was done sequentially with 30 keV, 5 keV and 2 keV Ga ions. Although the FIB process produced damage that could potentially be confused with radiation damage, neither cavities nor faulted dislocation loops were observed either in unirradiated samples prepared by FIB or in irradiated samples beyond the ion range. Because of this, these features could be characterized with confidence in the irradiated region as being created by ion irradiation.

Samples were characterized using JEOL 2010 and FEI Tecnai G2 transmission electron microscopes. Faulted dislocation loops were imaged with rel-rod dark-field imaging and cavities were imaged using under/over-focus imaging (see Ref. [12] for an overview of characterization techniques). The foil thickness (essential for quantitative determination of defect densities) was measured at one or more locations in each sample using convergent beam electron diffraction (CBED) [13] which was then used to calibrate energy filtered TEM (EFTEM) generated thickness maps.

When finding the density and average diameter of defects, the number counted (N) and the diameter of each individual defect (D_i) were directly measured from micrographs. The density (ρ) is calculated by

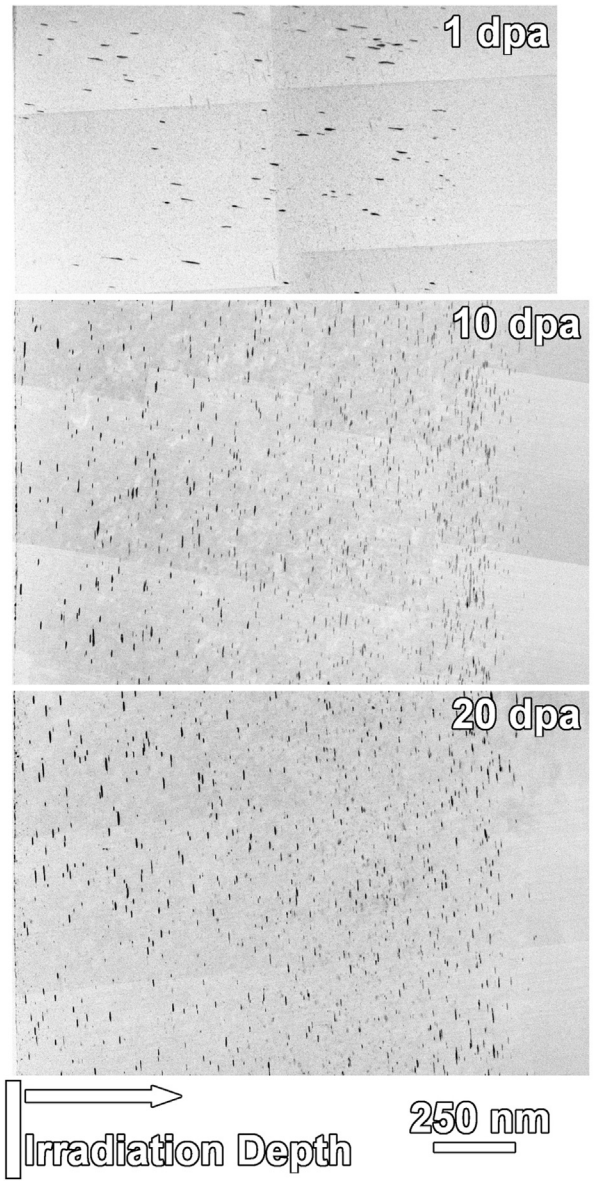

Fig. 5. Cross-sectional rel-rod dark-field TEM image of edge-on faulted dislocation loops in 800H after bulk ion irradiation to 1, 10, and 20 dpa showing the depth profile of the loops. The image contrast is inverted for easier viewing.

$$\rho = \frac{N}{V} \tag{1}$$

with the error (ε_ρ) equal to

$$\varepsilon_\rho = \rho\sqrt{\left(\frac{\varepsilon_N}{N}\right)^2 + \left(\frac{\varepsilon_t}{t}\right)^2} \tag{2}$$

where V is the characterized volume, ε_t is the error of the thickness measurement, taken as 10% of the measured thickness (t), and $\varepsilon_N = \sqrt{N}$ is the counting standard error. The average defect diameter $(\overline{D})$ is calculated by

$$\overline{D} = \frac{1}{N}\sum_{n=1}^{N} D_i \tag{3}$$

with the error (ε_D) given by

$$\varepsilon_D = \sqrt{\varepsilon_D^2 + \varepsilon_m^2} \tag{4}$$

where $\varepsilon_D = \sigma_D/\sqrt{N}$ is the standard error of the diameter measurements, σ_D is the standard deviation of the diameter measurements, and ε_m is the measurement error taken as the size of a pixel in the image. The confidence intervals shown with the measurements in later sections correspond to two times these standard errors [14].

Two additional in-situ irradiations of samples that were previously bulk-ion irradiated were performed at the Intermediate Voltage Electron Microscope (IVEM) facility at Argonne National Laboratory in order to study the dynamics of dislocation loop and cavity evolution with dose. TEM samples were produced from the 1 dpa and 10 dpa bulk ion irradiated material using FIB[2] and were irradiated in-situ with 1 MeV Kr^{2+} ions at 440 °C to additional doses. During the in-situ irradiation, the temperature was monitored continuously using a thermocouple attached to the sample cup and was found to remain within 3 °C of the target temperature. The microscope was operated at 200 keV. Assuming a displacement energy of 40 eV, the operating voltage is low enough such that carbon is the heaviest element that can be displaced directly, and the main constituent elements of iron, nickel, and chromium cannot be displaced by secondary collisions (i.e. the electron impacts a carbon atom which then impacts a metal atom) [15].

SRIM was again used to calculate the fluence-to-dpa ratio, which is 5.68×10^{18} ions/m^2 per 1 dpa for a 100 nm thick sample. The damage and implantation profiles are shown in Fig. 2(b). The 1 dpa sample was irradiated for an additional 4 dpa at an average dose rate of 1.0×10^{-3} dpa/s to a total of 5 dpa including the prior bulk ion irradiation, and the 10 dpa sample was irradiated for an additional 2 dpa at an average dose rate of 7.6×10^{-4} dpa/s to a total of 12 dpa, including the prior bulk ion irradiation. The dislocation microstructure was monitored in the 1 dpa sample using bright-field and dark-field diffraction contrast, and the cavities were monitored in the 10 dpa sample using underfocus imaging. The microstructure was followed during irradiation by continuously recording video and systematically acquiring both high quality still images and diffraction patterns while pausing the irradiations after chosen dose steps to continually optimize imaging conditions. No visible changes to the microstructure occurred during these pauses when the ion beam was turned off.

3. Results

3.1. Characterization of bulk ion irradiated samples

Images of the irradiated dislocation microstructure observed after doses of 1, 10 and 20 dpa were recorded near the target depth, 0.6 μm, as shown in the bright-field and dark-field micrographs in Fig. 3. After an irradiation dose of 1 dpa, the irradiated microstructure consists of dislocation loops, most of which were observed to be faulted and with an orientation consistent with a {111} habit plane. Application of the inside-outside technique for determining loop nature (see Ref. [12]) to a few of the loops indicated that they were interstitial in nature. The dislocation microstructures observed at 10 and 20 dpa appeared to be similar to one another and exhibited a higher dislocation density than that seen at 1 dpa. In addition to previously observed faulted loops with {111}

[2] Platinum deposition was used instead of carbon for FIB preparation of these samples.

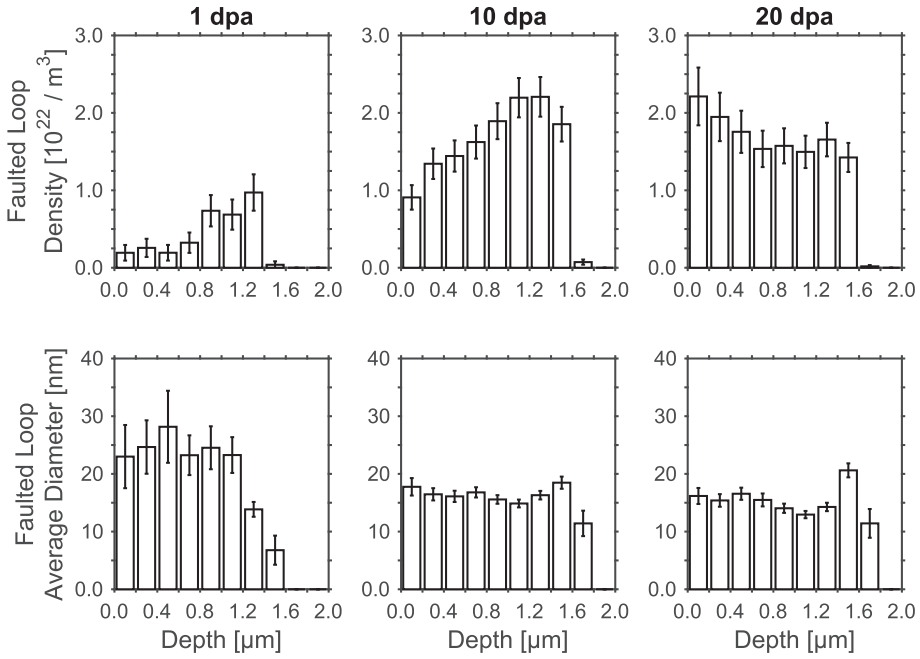

Fig. 6. Faulted loop density and faulted loop average diameter measured as a function of depth for 800H irradiated to 1, 10 and 20 dpa at 440 °C.

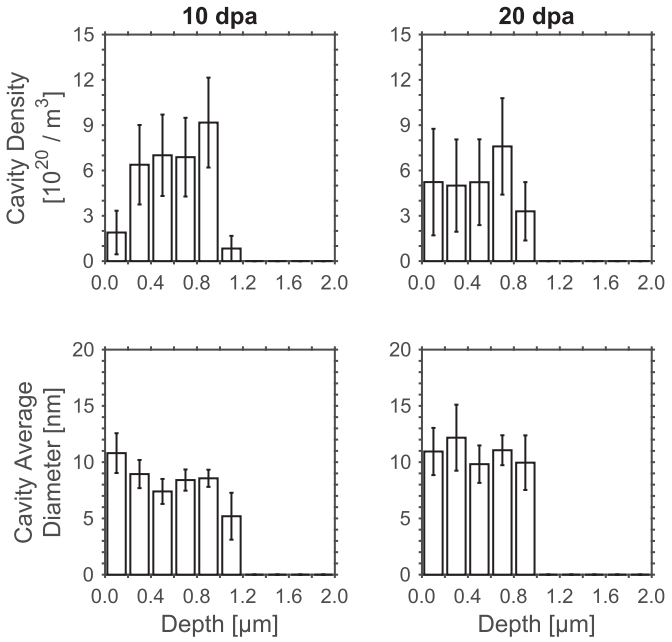

Fig. 7. Cavity density and cavity average diameter measured as a function of depth for 800H irradiated to 10 and 20 dpa at 440 °C. No cavities were observed at 1 dpa.

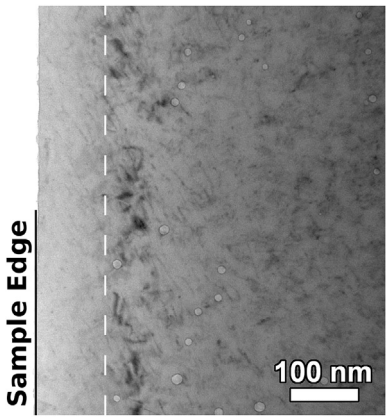

Fig. 8. A bright-field TEM image showing the cavity denuded zone observed near the surface during bulk ion irradiation. This image was acquired at 1 μm underfocus after irradiation to 10 dpa, and the area without cavities is marked by the dotted line.

habit plane, a dislocation network formed, likely from the growth and coalescence of dislocation loops occurring between the doses of 1 and 10 dpa. Cavities were also observed at 10 and 20 dpa, but were not observed at 1 dpa.

Faulted dislocation loops on {111} habit planes were characterized using rel-rod dark-field imaging (see Fig. 4 for an example). These rel-rods originate from the stacking faults of the faulted dislocation loops and are oriented perpendicular to the habit plane of the loops. A series of images were recorded at moderate magnification (30kx and 35kx) and stitched together to form images showing the majority of an irradiated sample's area, as shown in Fig. 5. Each dislocation loop was marked using ImageJ [16] and then the position and diameter of each loop was measured. This procedure was performed for two distinct crystallographic variants of edge-on faulted {111} loops in each sample which can be observed near the [110] zone axis. The faulted loop density and average diameter were calculated at each dose as a function of depth and are shown in Fig. 6. The faulted loop density shown in Fig. 6 corresponds to the sum of the two measured variants multiplied by two to account for the other two variants that were not measured.

At 1 and 10 dpa the faulted loop density appeared to be proportional to the depth-dependence of radiation dose such that higher doses resulted in greater faulted loop density with the maximum dose at approximately 1.3 μm. At 20 dpa, the faulted loop density appeared to saturate in the depth region of 0.4–1.6 μm where the faulted loop density varied weakly with depth (and correspondingly dose variation with depth). The faulted loop density did appear higher at less than 0.4 μm depth than beyond that

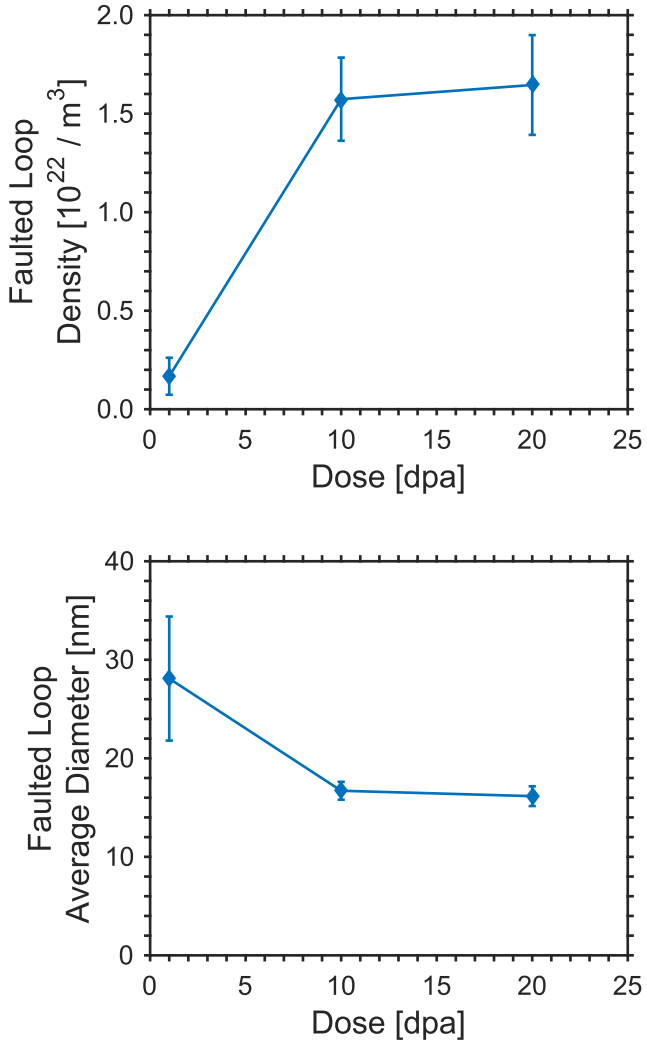

Fig. 9. Faulted loop density and faulted loop average diameter as functions of dose for the depth range of 0.5–0.7 μm.

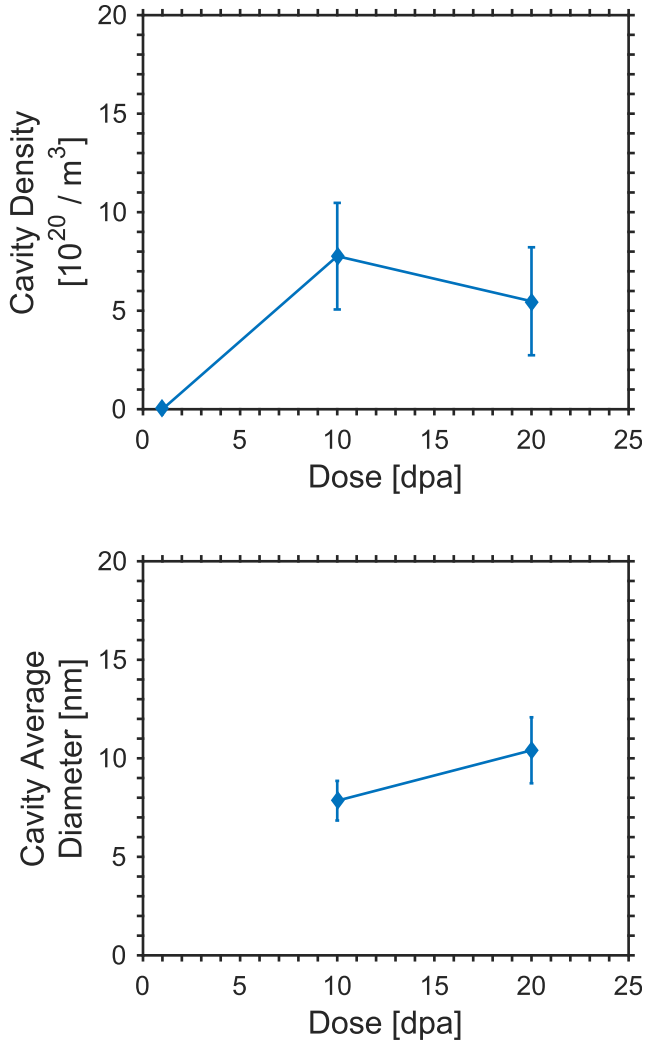

Fig. 10. Cavity density and cavity average diameter as functions of dose for the depth range of 0.5–0.7 μm.

depth, which suggests that the presence of the irradiated surface affected the faulted loop density.

Overall, the faulted loop average diameter decreased from 1 dpa to 10 dpa and then decreased little with further irradiation to 20 dpa. Few loops were available for measurement at 1 dpa and as a consequence no statistically significant trend could be determined for the depth dependence of faulted loop average diameter. After an irradiation dose of 1 dpa, the diameter of the loops observed beyond a depth of 1.2 μm, near the ion penetration range, was significantly lower than those seen at shallower depths and may simply be due to higher local dose. After irradiation doses of 10 and 20 dpa, the average diameter of the faulted loops did not vary significantly with either depth or dose, although at 20 dpa a band of larger faulted loops was observed near the ion implantation peak at a depth of 1.4–1.6 μm.

A similar depth-dependent analysis was carried out for cavities. The micrographs were recorded at the same magnifications as for the faulted loops, and the cavities were imaged using 1 μm underfocus in a highly kinematical bright-field diffraction condition. The diameters were measured to the inside of the dark fringe. Although cavities were not observed after an irradiation dose of 1 dpa, a fair number were observed after doses of 10 and 20 dpa. The depth dependences of cavity density and cavity average diameter at 10 and 20 dpa are shown in Fig. 7.

No cavities were observed beyond a depth of 1.2 μm, likely due to the fact that at this depth ion implantation created an excess of interstitials which suppressed cavity formation. No cavities were observed within 100 nm of the irradiated surface, and this cavity denuded zone is shown in Fig. 8. This suggests that the presence of the free surface suppresses cavity formation which would be in agreement with the cavity instability seen later during in-situ irradiation. No statistically significant trends of cavity density with depth were observed in the remaining region of the sample, and the cavity average diameter was also approximately constant with depth.

The density and diameter of faulted dislocation loops and of cavities was analyzed for the depth region near the depth of the target dose, 0.5–0.7 μm. The density and average diameter of these loops as a function of dose is plotted in Fig. 9, and the same for cavities in Fig. 10. The error bars are calculated as described with Eq. (2) and Eq. (4), and the values are also provided in Table 3. The faulted loop density increased from $(1.7\pm0.9)\times10^{21}$ m^{-3} after 1 dpa irradiation to $(1.6\pm0.2)\times10^{22}$ m^{-3} after 10 dpa. The density changed little between 10 and 20 dpa where it reached $(1.6\pm0.3)\times10^{22}$ m^{-3}. The faulted loop average diameter, on the other hand, decreased from 28.1±6.3 nm at 1 dpa to 16.7±0.9 nm at 10 dpa and

Table 3
Density and average diameter measurements for faulted dislocation loops and cavities at 0.5–0.7 μm depth after bulk ion irradiation by 5 MeV Fe^{2+} ions. No cavities were observed at 1 dpa.

Dose dpa	Faulted Loop Density m^{-3}	Faulted Loop Avg. Diameter nm	Cavity Density m^{-3}	Cavity Avg. Diameter nm
1	$(1.7\pm0.9)\times10^{21}$	28.1±6.3	–	–
10	$(1.6\pm0.2)\times10^{22}$	16.7±0.9	$(7.8\pm2.7)\times10^{20}$	7.8±1.0
20	$(1.6\pm0.3)\times10^{22}$	16.2±1.0	$(5.5\pm2.7)\times10^{20}$	10.4±1.7

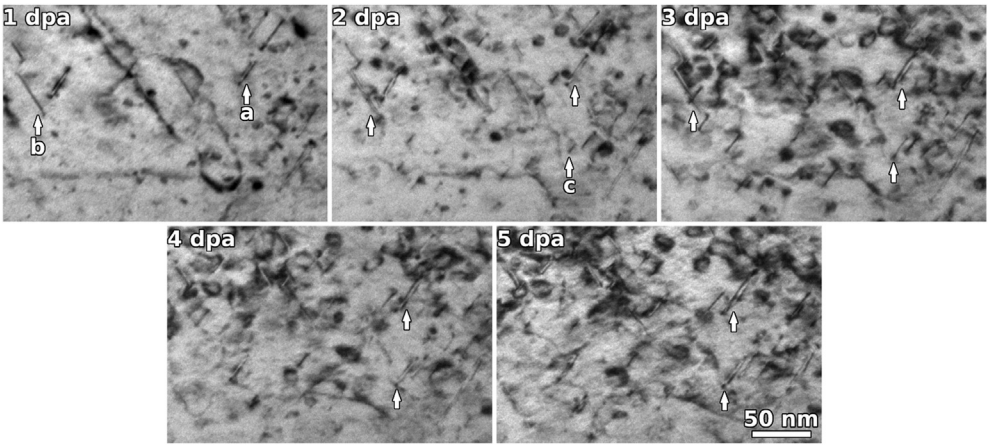

Fig. 11. Bright-field TEM micrographs of dislocations in 800H after bulk ion irradiation to 1 dpa at 440 °C followed by 4 dpa in-situ ion irradiation at 440 °C to 5 dpa combined dose. The images were acquired using a $g = 002$ kinematical diffraction condition near the [110] zone axis and are labeled using the combined bulk and in-situ dose. Arrow "a" indicates a loop that remained throughout the in-situ irradiation, arrow "b" shows a loop that unfaulted during irradiation, and arrow "c" points to a loop that formed and grew during irradiation.

remained approximately constant after 20 dpa (16.2±1.0 nm).

No cavities were observed after an irradiation dose of 1 dpa. After 10 dpa the cavity density was $(7.8\pm2.7)\times10^{20}$ m^{-3} decreasing to $(5.5\pm2.7)\times10^{20}$ m^{-3} at 20 dpa. Due to the low number of cavities, these two measured densities are within experimental error. The cavity average diameter did however increase from 7.8±1.0 nm after 10 dpa to 10.4±1.7 nm at 20 dpa. The total swelling is calculated to be 0.028±0.015% after 10 dpa and 0.042±0.028% after 20 dpa, approximately doubling with a doubling of the dose.

3.2. In-situ ion irradiation of bulk ion irradiated samples

A significant change in dislocation microstructure occurred between 1 and 10 dpa during bulk ion irradiation. In order to better understand the microstructure evolution under irradiation, a FIB sample was created from 800H after bulk ion irradiation to 1 dpa at 440 °C, and re-irradiated in-situ at 440 °C using the IVEM for an additional 4 dpa. Sample bending at the irradiation temperature prevented the use of precise diffraction conditions, but a kinematic $g = 002$ bright-field diffraction condition was maintained throughout the experiment to observe the dislocation structure. A series of images showing the same location in the sample with increasing dose is shown in Fig. 11. The dislocation loops already present in the sample before in-situ irradiation (see loops "a" and "b" in Fig. 11) either grew with dose or stayed the same size. Additionally, new dislocation loops formed during in-situ irradiation, all of which grew with additional dose (loop "c" in Fig. 11). Some of the large dislocation loops appeared to transform and incorporate into a network dislocation structure, possibly through an unfaulting process (loop "b" in Fig. 11 between 3 and 4 dpa).

Ten edge-on dislocation loops, including a mixture of those present before in-situ irradiation and those formed during in-situ irradiation, were measured after each dose step. The diameters of the individual loops followed as functions of dose are shown for each loop in Fig. 12(a). The average time rate of change of loop diameter as a function of dose was calculated for each dose step and plotted in Fig. 12(b). Although the loop size increased with dose, the loop growth rate decreased from nearly 12 nm/dpa during the first dose step to approximately 2 nm/dpa during the final dose step. It could be that the higher dislocation density and subsequent sink strength at higher doses suppressed the number of point defects available for individual loops to grow. Also, as loops grow a larger number of defects is needed to increase the loop diameter by a given amount.

Because no cavities were seen under in-situ ion irradiation, it was of interest to examine the behavior of cavities formed during bulk irradiation when subjected to further ion irradiation in-situ. For that purpose, a FIB sample created from 800H after bulk ion irradiation to 10 dpa at 440 °C was irradiated in-situ using the IVEM for an additional 2 dpa at 440 °C. The cavities present in the sample were monitored using underfocus, kinematic bright-field conditions.

The cavity microstructure as a function of dose is shown in Fig. 13. Interestingly, the cavities formed under bulk ion irradiation were found to shrink and disappear during in-situ irradiation, i.e. their diameters decreased with dose. In Fig. 13, the cavity marked "a" shows a cavity that shrank but was still visible after a further 2 dpa, while the cavity marked "b" had completely disappeared after a further 2 dpa in-situ. Cavity diameter was measured as function of dose in this manner for forty-five individual cavities as shown in Fig. 14(a). Additionally, the rate of change of cavity diameter is shown as a function of cavity diameter in Fig. 14(b). The rate of change of cavity diameter was highest for smaller cavities, which is expected because larger cavities need to absorb more defects to change their diameter by a fixed amount than for smaller cavities.

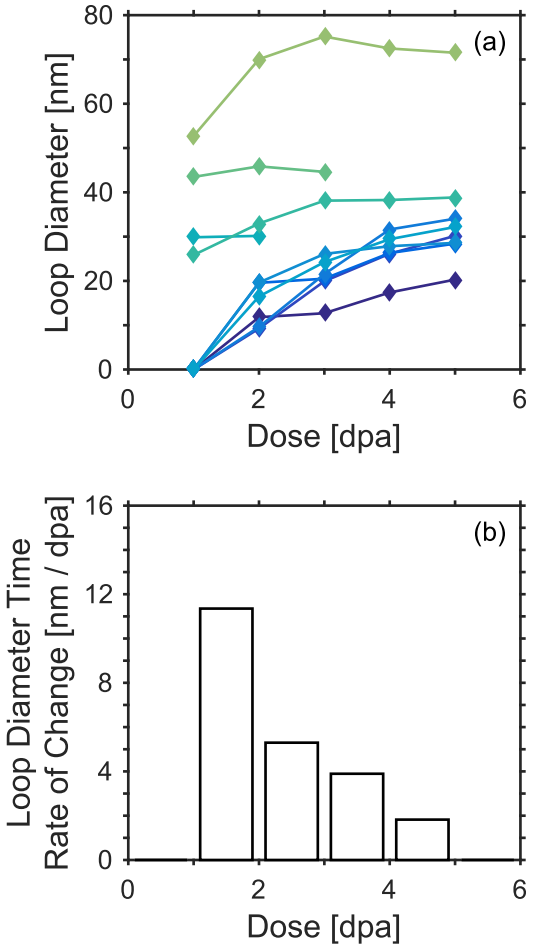

Fig. 12. (a) Dose dependent measurements of ten edge-on loop diameters during in-situ irradiation of 800H at 440 °C after bulk irradation to 1 dpa. (b) The time rate of change of loop diameter calculated as an average over all loops shown in the upper figure for a given dose step.

Finally we note that the cavity shrinkage was only observed during irradiation; no shrinkage was observed when the sample was simply held at temperature for approximately 30 min prior to the start of irradiation. Norris [17] also found that annealing a stainless steel thin-foil showed no significant void shrinkage even after 5 h at 650 °C without the electron beam.

4. Discussion

Bulk ion irradiation of 800H at 1, 10 and 20 dpa revealed the evolution of dislocation microstructure with dose. At 1 dpa, the dislocation structure was still in a state of fast evolution and consisted mainly of {111} faulted dislocation loops. The density of faulted loops increased significantly as the dose was increased to 10 dpa, but the average diameter of the faulted loops decreased. In addition to the changes in loop population, a network dislocation structure formed during irradiation. Both of these results are consistent with systematic unfaulting of the loops as they grow and their coalescence into a dislocation network. The dislocation structure did not significantly change between 10 and 20 dpa, indicating a possible saturation of dislocation structure including loop size and density. If this trend continued then only small modifications of the dislocation microstructure with additional dose beyond 20 dpa would be expected.

The evolution of austenitic stainless steel microstructure under

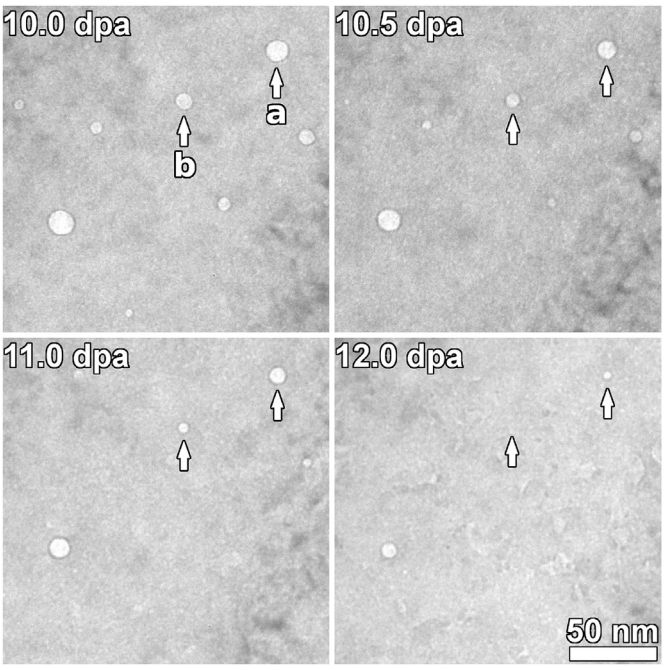

Fig. 13. Bright-field TEM micrographs of cavities in 800H after bulk ion irradiation to 10 dpa at 440 °C followed by 2 dpa in-situ ion irradiation at 440 °C to 12 dpa combined dose. The images were acquired using a highly kinematical diffraction condition at 1 μm underfocus and are labeled using the combined bulk and in-situ dose. Cavity "a" shrank but remained after in-situ irradiation while cavity "b" completely shrank and disappeared during in-situ irradiation.

irradiation is reviewed in Ref. [2]. At the irradiation temperature used in this work, faulted dislocation loops nucleate and grow first. Impingement of faulted loops can result in unfaulting of the loop(s) and incorporation into the dislocation network. This behavior agrees with the observations made during this work, as outlined in the previous paragraph. The unfaulting mechanisms for Frank loops, reviewed in Ref. [18], in general include an unfaulting interaction with a Shockley partial dislocation resulting from motion of a glissile dislocation or by nucleation of a Shockley partial in the Frank loop.

Further in-situ irradiation of a FIB lift-out taken from the 1 dpa bulk ion irradiated sample showed new dislocation loops forming and existing dislocation loops growing. Additionally, some dislocation loops reacted and became part of a dislocation network. These results indicate that even though faulted loop average diameter decreased from 1 to 10 dpa during bulk ion irradiation, it is unlikely that individual loops shrank. It is more likely that the incorporation of large loops into the dislocation network and the formation of new small loops during irradiation resulted in the decrease in the measured faulted loop average diameter, as observed during the in-situ irradiation. The dislocation density during the in-situ irradiations was high such that it was difficult to know the exact unfaulting mechanisms that occurred. The unfaulting appeared to occur through interaction with other dislocations.

Cavities were not observed after 1 dpa bulk irradiation, but were observed after 10 and 20 dpa. The average cavity diameter increased with dose from 10 to 20 dpa suggesting a supersaturation of vacancies was available for cavity growth. Calculation shows that total swelling increased with dose, from 0.028% after 10 dpa to 0.042% after 20 dpa, as has been seen for austenitic stainless steels [2].

The cavities formed during 10 dpa bulk ion irradiation shrank

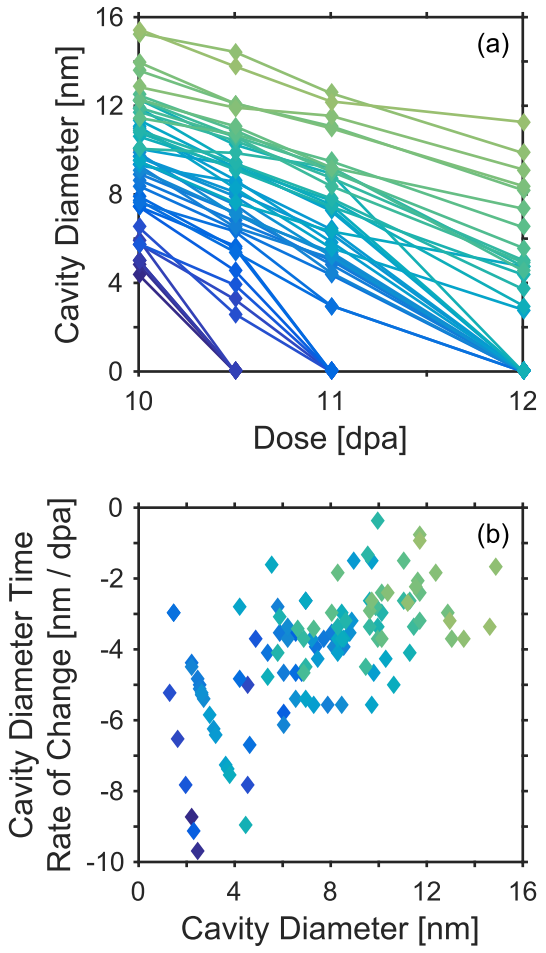

Fig. 14. (a) Dose dependent measurements of forty-five individual cavities during in-situ irradiation of 800H at 440 °C following bulk irradation to 10 dpa. (b) The time rate of change of cavity diameter is plotted against the cavity diameter for each cavity and dose step.

during in-situ re-irradiation. This is in marked contrast to bulk ion irradiation to 20 dpa where the average cavity diameter was observed to increase with additional dose. The growth of the average diameters from 10 to 20 dpa during bulk ion irradiation implies a net flux of point defects, *vacancies minus interstitials*, of +1.5 per second. The net flux is calculated by the equation

$$J = \frac{\pi\left(d_f^3 - d_i^3\right)}{6\Omega\Delta t} \tag{5}$$

where J is the net flux of point defects, d is the cavity diameter at the initial (i) and final (f) dose points, Ω is the atomic volume, and Δt is the time of irradiation. In contrast, the net flux necessary to account for the observed shrinkage during in-situ re-irradiation was −22.2 per second on average for each individual cavity and dose step.[3] This is a total difference of −23.7 per second when switching from bulk ion irradiation to in-situ ion irradiation. We note that in-situ irradiation of virgin material caused no cavity formation. This indicates that cavities were unstable during thin-foil irradiation. Some mechanisms that can produce this result are discussed.

Because two different ion species and ion energies are used, 5 MeV Fe^{2+} for bulk ion irradiation and 1 MeV Kr^{2+} for in-situ ion irradiation, there are different rates of ion implantation. Additional ion implantation might suppress the vacancy concentration by enhancing recombination. The numbers of implanted ions for both irradiations are found using SRIM at 0.6 μm depth for bulk ion irradiation and averaged over the entire 100 nm foil thickness for in-situ ion irradiation. The in-situ irradiation implants just over twice the number of ions than does bulk irradiation to reach the same dose level.

To find the maximum possible effect of implanted ions on cavities, it is assumed that every implanted ion causes an additional recombination that prevents a vacancy from reaching a cavity. By dividing the rate of ion implantation by the cavity density, this effect is evaluated on a per-cavity basis. Using the cavity density at 10 dpa, 7.8×10^{20} m^{-3}, this calculation shows that in-situ irradiation implants more ions per cavity than bulk ion irradiation with a difference in rate of 1.6 implanted ions per cavity per second. While this value alone is large enough to offset the estimated rate of growth of cavities during bulk ion irradiation, thus potentially causing cavities to stop growing, it would not account for the fast shrinkage of cavities observed during in-situ ion irradiation.

Cavity formation was seen to be affected by the proximity of the irradiated surface as evidenced by the cavity denuded zone near the surface of the bulk ion irradiated material. This suggests that the nearby sample surface suppresses cavity formation and growth, possibly by the same mechanisms that causes cavities to shrink during in-situ irradiation. Such interaction of defects with the foil surface has also been observed previously, for example by Garner et al. where, after an initial neutron irradiation, 300 series stainless steel was irradiated by electrons in a high-voltage electron microscope (HVEM) and cavity denuded zones formed near the foil

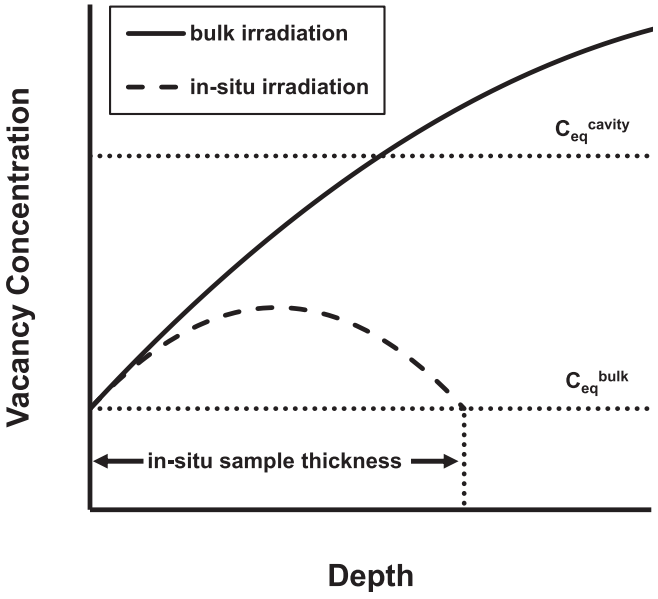

Fig. 15. A schematic diagram showing the action of the sample surface as a defect sink and its effect on the vacancy concentration profiles during in-situ and bulk ion irradiation. The vacancy concentration at the surface is the thermal equilibrium value in the bulk material, C_{eq}^{bulk}, and the concentration increases away from the surface as new defects are constantly produced during irradiation. In order for cavities to be stable, the vacancy concentration must be greater than the equilibrium vacancy concentration around the cavities, C_{eq}^{cavity}. This example suggests how a cavity-free zone could form near the surface during bulk-irradiation and how no cavities could form, or even remain stable, during in-situ irradiation.

[3] The net flux of vacancies to cavities during in-situ irradiation is between 1/1000 and 1/10,000 of the rate of Frenkel pair production as calculated by SRIM. This suggests that the cavities are a small contribution to the total sink strength for point defects.

surfaces as identified by stereomicroscopy [19]. Norris [17] also reported void denuded regions in nickel and stainless steel at thin-foil surfaces during HVEM irradiation.

Because the surface acts as a sink for defects, thin samples used for in-situ ion irradiation are likely to have lower mobile defect concentrations than bulk ion irradiation. In this scenario, both defects, interstitials and vacancies, would be mobile enough to get to the surface. If the vacancy concentration was decreased to or below the equilibrium vacancy concentration around the cavities such that there is negligible absorption of vacancies, or even some emission of vacancies, from the cavities (see the schematic in Fig. 15), then the interstitial flux into each cavity would shrink them. This process would be much faster than the thermal dissolution of cavities by vacancy emission, and, importantly, would only occur under irradiation.

These results suggest that in-situ irradiation is not an appropriate means of directly reproducing the irradiated microstructure, in particular cavity formation. Rather, in-situ irradiation should be seen and used as an alternative way to subject the sample to irradiation and thus allow us to investigate the dynamics of defect formation and aggregation under different conditions. It seems clear that the thin-foil geometry greatly affects the behavior of cavities during irradiation [17,19]. However, in-situ irradiation should instead be used for observation of dynamic defect interactions and detailed kinetics of microstructure evolution. For example, during bulk irradiation it is not possible to follow the growth of an individual defect or observe the unfaulting of a loop, both of which are possible using in-situ irradiation and provide additional insights into the mechanisms of microstructural evolution.

5. Conclusion

A detailed characterization of the microstructure of 800H bulk ion irradiated to 1, 10 and 20 dpa at 0.6 μm depth was performed using TEM. The size and density of faulted dislocation loops on {111} planes and cavities were measured as functions of depth from the irradiated surface. At 1 and 10 dpa, the faulted loop density was nominally proportional to the local dose, but that trend did not continue at 20 dpa where density saturation possibly occurred. The faulted loop diameter depended weakly on depth. At the depth of 0.6 μm, where the surface and implantation was minimal, the density of faulted loops increased with dose from 1.7×10^{21} m^{-3} at 1 dpa up to 1.6×10^{22} m^{-3} at 10 and 20 dpa at which point the density of faulted loops had saturated. The average diameter of those loops, however, decreased with dose from 28.1 nm at 1 dpa to 16.7 nm and 16.2 nm at 10 and 20 dpa, respectively. Cavities were not observed after irradiation to 1 dpa, but did appear after irradiation to 10 and 20 dpa. While cavity density showed a slight decrease from 7.8×10^{20} m^{-3} at 10 dpa to 5.5×10^{20} m^{-3} at 20 dpa, the average cavity diameter increased from 7.8 to 10.4 nm. Cavities were not observed near the irradiated surface nor near the ion implantation peak.

Additional in-situ ion irradiation was performed on FIB lift-out samples taken from the 1 and 10 dpa bulk ion irradiated material. The dislocation microstructure was followed in the 1 dpa sample as it was irradiated to an additional 4 dpa. New dislocation loops formed, and existing loops increased in diameter with further irradiation. The rate at which existing loops grew decreased as the dose increased. Some loops were integrated into a network dislocation microstructure through what appears to be a loop unfaulting process. The cavity microstructure observed in the sample irradiated to 10 dpa was given an additional 2 dpa of in-situ irradiation. The cavities formed during bulk irradiation were observed to shrink upon in-situ re-irradiation and many disappeared completely by the final dose point. Estimates indicate that ion implantation could not account for the rate at which cavities shrank, and it is believed that the loss of mobile vacancy defects to the surfaces of the thin foil contributed to this observation.

Acknowledgments

This work was funded by the U.S. Department of Energy's Nuclear Engineering University Program Integrated Research Project on High Fidelity Ion Beam Simulation of High Dose Neutron Irradiation under award number DE-NE0000639. We thank Gary Was and Stephen Taller of the Michigan Ion Beam Laboratory for providing the bulk ion irradiated samples. The electron microscopy with in-situ ion irradiation was accomplished at Argonne National Laboratory at the IVEM-Tandem Facility, a U.S. Department of Energy Facility funded by the DOE Office of Nuclear Energy, operated under Contract No. DE-AC02-06CH11357 by UChicago Argonne, LLC. We thank Mark Kirk, Pete Baldo, and Ed Ryan of Argonne National Laboratory for their invaluable assistance in carrying out the in-situ irradiations.

References

[1] ASTM B409-06, Standard Specification for Nickel-iron-chromium Alloy Plate, Sheet, and Strip, ASTM International, 2016, https://doi.org/10.1520/B0409-06R16.
[2] S.J. Zinkle, P.J. Maziasz, R.E. Stoller, J. Nucl. Mater. 206 (1993) 266–286, https://doi.org/10.1016/0022-3115(93)90128-L.
[3] G. Lucas, J. Nucl. Mater. 206 (1993) 287–305, https://doi.org/10.1016/0022-3115(93)90129-M.
[4] G.S. Was, Z. Jiao, E. Getto, K. Sun, A.M. Monterrosa, S.A. Maloy, O. Anderoglu, B.H. Sencer, M. Hackett, Scr. Mater. 88 (2014) 33–36, https://doi.org/10.1016/j.scriptamat.2014.06.003.
[5] J. Gan, J.I. Cole, T.R. Allen, S. Shutthanandan, S. Thevuthasan, J. Nucl. Mater. 351 (2006) 223–227, https://doi.org/10.1016/j.jnucmat.2006.02.009.
[6] J. Gan, B.A. Hilton, TEM Examination of Advanced Alloys Irradiated in ATR, Technical Report INL/EXT-07–13306, Idaho National Laboratory (INL), 2007.
[7] L. Tan, J.T. Busby, H.J.M. Chichester, K. Sridharan, T.R. Allen, J. Nucl. Mater. 437 (2013) 70–74, https://doi.org/10.1016/j.jnucmat.2013.01.333.
[8] R.K. Nanstad, D.A. McClintock, D.T. Hoelzer, L. Tan, T.R. Allen, J. Nucl. Mater. 392 (2009) 331–340, https://doi.org/10.1016/j.jnucmat.2009.03.022.
[9] L. Mansur, J. Nucl. Mater. 206 (1993) 306–323, https://doi.org/10.1016/0022-3115(93)90130-Q.
[10] J.F. Ziegler, M. Ziegler, J. Biersack, Nucl. Instrum. Methods Phys. Res. Sect. B Beam Interact. Mater. Atoms 268 (2010) 1818–1823, https://doi.org/10.1016/j.nimb.2010.02.091.
[11] R.E. Stoller, M.B. Toloczko, G.S. Was, A.G. Certain, S. Dwaraknath, F.A. Garner, Nucl. Instrum. Methods Phys. Res. Sect. B Beam Interact. Mater. Atoms 310 (2013) 75–80, https://doi.org/10.1016/j.nimb.2013.05.008.
[12] M.L. Jenkins, M.A. Kirk, Characterization of Radiation Damage by Transmission Electron Microscopy, Series in Microscopy in Materials Science, Institute of Physics Publishing, 2001.
[13] P.M. Kelly, A. Jostsons, R.G. Blake, J.G. Napier, Phys. Status Solidi (A) 31 (1975) 771–780, https://doi.org/10.1002/pssa.2210310251.
[14] R. Lock, P. Lock, K. Morgan, E. Lock, D. Lock, Statistics: Unlocking the Power of Data, 2 ed., John Wiley & Sons, 2017.
[15] O. Oen, Cross Sections for Atomic Displacements in Solids by Fast Electrons, Technical Report, Oak Ridge National Laboratory, 1973. Report # 4897.
[16] C.A. Schneider, W.S. Rasband, K.W. Eliceiri, et al., Nat. Methods 9 (2012) 671–675, https://doi.org/10.1038/nmeth.2089.
[17] D. Norris, J. Nucl. Mater. 40 (1971) 66–76, https://doi.org/10.1016/0022-3115(71)90117-6.
[18] E. Lee, M. Yoo, T. Byun, J. Hunn, K. Farrell, L. Mansur, Acta Mater. 49 (2001) 3277–3287, https://doi.org/10.1016/S1359-6454(01)00194-X.
[19] F.A. Garner, J.J. Laidler, B. Mastel, L.E. Thomas, ASTM STP 570, 1975, pp. 433–448, https://doi.org/10.1520/STP33705S.